FGF2 and BMP4 influence on FGFR2 dynamics during the segregation of epiblast and primitive endoderm cells in the pre-implantation mouse embryo

Marcelo D. Goissis[1,3], Brian Bradshaw[1], Eszter Posfai[1,4], Janet Rossant[1,2]

[1]Program in Developmental and Stem Cell Biology, The Hospital for Sick Children, Toronto, ON, Canada

[2] Department of Molecular Genetics, University of Toronto

Corresponding Author: Janet Rossant
Hospital for Sick Children Research Institute
686 Bay Street
Toronto
Ontario
Canada M5G 0A4
Email: janet.rossant@sickkids.ca

[3]Current Address: Department of Animal Reproduction, College of Veterinary Medicine and Animal Science, University of Sao Paulo, Brazil

[4]Current Address: Princeton University, Department of Molecular Biology, Princeton, NJ, USA

Short title: FGF and BMP signaling and primitive endoderm differentiation

Abstract

Specification of the epiblast (EPI) and primitive endoderm (PE) in the mouse embryo involves FGF signaling through the RAS/MAP kinase pathway. FGFR1 and FGFR2 are thought to mediate this signaling in the inner cell mass (ICM) of the mouse blastocyst. In this study, we verified the dynamics of FGFR2 expression through a green fluorescent protein reporter mouse line (FGFR2-eGFP). We observed that FGFR2-eGFP is present in the late 8-cell stage; however, it is absent or reduced in the ICM of early blastocysts. We then correlated GFP expression with GATA6 and NANOG after immunostaining. We detected that GFP is weakly correlated with GATA6 in early blastocysts, but this correlation quickly increases as the blastocyst develops. The correlation between GFP and NANOG decreases throughout blastocyst development. Treatment with FGF from the morula stage onwards did not affect FGFR2-eGFP presence in the ICM of early blastocysts; however, late blastocysts presented FGFR2-eGFP in all cells of the ICM. BMP treatment positively influenced FGFR2-eGFP expression and reduced the number of NANOG-positive cells in late blastocysts. In conclusion, FGFR2 is not strongly associated with PE precursors in the early blastocyst, but it is highly correlated with PE cells as blastocyst development progresses, consistent with the proposed role for FGF in maintenance rather than initiating the PE lineage.

Introduction

After fertilization, a series of coordinated events must occur to form an embryo capable of implanting and developing in the uterus. These early events in mammals are characterized by a self-organizing, regulative mode of development (1). During a short period, cells first differentiate into the inner cell mass (ICM) and the trophectoderm (TE), followed by a second differentiation within the ICM into epiblast (EPI) and primitive endoderm (PE). The epiblast will give rise to the embryo proper, while PE will form extra-embryonic endoderm of the visceral and parietal yolk sacs (2,3)

Epiblast cells express NANOG, while PE cells first express GATA6, followed by SOX17, GATA4, and PDGFR (4–6). The blastocyst forms around embryonic day 3.25 (E3.25) and at this time ICM cells express both NANOG and GATA6 (5,7). As the blastocyst further develops, NANOG and GATA6 expression become mutually exclusive in EPI and PE progenitors, respectively (5,8), and eventually, the PE progenitors will migrate towards the blastocoel cavity to form the PE layer (5). It was shown that both Nanog and Gata6 mutually repress each other, as *Nanog*-null embryos led to the expression of GATA6 in all ICM cells (9) while *Gata6*-null embryos display NANOG in all ICM cells (10,11). Interestingly, PE did not form in Nanog-null embryos, as observed by the lack of SOX17 and GATA4, which was caused by a reduction in the expression of *Fgf4* (9).

Fibroblast-growth factor signaling through MEK/ERK is central in establishing PE. Deletion of *Grb2* blocked the formation of the PE and led to the expression of NANOG in all ICM cells (4). Inhibition of the MEK/ERK

pathway or treatment with excess FGF4 changed the fate of all ICM cells to EPI or PE, respectively (12). This shift in cell fate was reversible if inhibition or activation of the FGF-mediated MEK/ERK signaling occurred before E3.75 (12). In addition, deletion of *Fgf4* caused all cells of the ICM to become NANOG-positive at E4.5, although GATA6 was still observed in earlier stages, suggesting that the PE program initiates independently of FGF signaling but requires sustained FGF exposure for lineage choice (7).

There is evidence that MEK/ERK signaling is required for phosphorylation and subsequent degradation of NANOG (13). Thus, an interesting question that still poses is how the initial double-positive NANOG and GATA6 cells respond differently to FGF signaling. It has been shown that *Fgfr2*-null embryos died soon after implantation and failed to form a yolk sac (14). Single-cell transcriptome analysis revealed that *Fgfr2* was more highly expressed in PE progenitors than in EPI progenitors in E3.5 mouse blastocysts, while expression of *Fgfr1* was similar in both. Expression of *Fgfr3* and *Fgfr4* was also found to be higher in PE cells but only at the later development stage E4.5 (15). Together, this data suggests that FGFR2 is essential for the differential response of ICM cells in the early blastocyst. However, mutational studies suggested that FGFR1 was critical for establishing the PE lineage, with FGFR2 playing a later role in the maintenance and stability of PE (16,17).

Since FGFR1 is present in all ICM cells (16,17), what leads to the specific expression of FGFR2 in PE precursors? It was published that p38 activation under the control of FGF4 participates in PrE specification before the E3.75 time point (18). The authors also showed a role for non-canonical

BMP signaling in the control of p38. Earlier, it was shown that inhibition of BMP signaling would impact the formation of PrE (19), although not as dramatically as MEK inhibition (12). In addition, single-cell transcriptome analysis revealed concomitant increase in BMP4, FGF4, NANOG, and SOX2 expression in putative epiblast cells (Guo *et al.* 2010).

We then hypothesized that FGF4 and BMP4 positively influence FGFR2 expression in PE progenitors. In this study, we used live imaging of FGFR2-eGFP embryos to verify the spatio-temporal dynamics of FGFR2 expression and observed that in early blastocysts, FGFR2 was not detectable in the ICM. We observed an increase in the correlation value between FGFR2 and GATA6 starting at the early blastocyst stage and continuing through to the mid and late blastocyst stage. This pattern is accompanied by an observed decrease in the correlation between NANOG and both FGFR2 and GATA6. Experiments with either exogenous FGF4 or MEK inhibitors from morula (E2.5) onwards did not influence the expression of FGFR2 in early blastocysts (E3.25), but respectively increased or decreased the number of FGFR2 positive cells at E3.5 and E4.5 embryos. Treatment with BMP4 from morula up to E4.5 decreased the number of NANOG positive cells and revealed a high correlation between FGFR2 and SOX17. Our results are consistent with a role for FGFR2 in maintenance but not initiation of the PE lineage.

Material and Methods

All animal work was performed following Canadian Council on Animal Care Guidelines for Use of Animals in Research and Laboratory Animal Care under Animal Use Protocol number 20–0026H, approved by The Centre for Phenogenomics Animal Care Committee.

FGFR2-eGFP mice generation

G4 Mouse ES cells (129S6/SvEvTac x C57BL/6Ncr, George *et al.* 2007) were used to knock-in eGFP downstream of the endogenous FGFR2 gene. The targeting plasmid was constructed using a custom designed and synthetized plasmid backbone containing a P2A-eGFP-SV40 NLS insert followed by FRT-SV40pA-PGK promoter-Neo-bGHpA-FRT (Biobasics). 4.8 (5') and 3 kb (3') homology arms for Fgfr2 were amplified from a BAC clone (RP23-332B13) and cloned into the targeting construct (homology arm and insert sequence provided in Supplementary files S1 and S2). ES cells were electroporated with the linearized targeting construct, Neomycin-selected, and clonally expanded. Individual clones were genotyped using over the arm PCR and single copy integration was validated using Southern blotting. Cells were then aggregated with a host morula (CD-1 background) to generate chimeras and transferred into pseudopregnant females. Resulting founder mice were identified by coat color chimerism and bred for germ line transmission. F1 animals were subsequently genotyped, and crossed to FlpE expressing mice to delete the Neomycin selection cassette (B6.Cg-Tg(ACTFLPe)9205Dym/J, Rodríguez *et al.* 2000). Mice were bred until homozygous.

149

150 **Embryo collection and culture**

151

152 Mice were superovulated after administration 5IU of eCG (PMSG) I.P.
153 between 11:00h and 13:00h and 46-48h later, administering 5IU of hCG I.P.
154 to induce ovulation. Females were immediately placed with studs after hCG
155 injection. Around 8:00h next morning, females were checked for successful
156 mating based on vaginal plug observation and were then separated from
157 males. Mating was considered to have occurred at 00:00h, which
158 characterizes embryonic day 0 (E0.0). Females were euthanized by cervical
159 dislocation at E0.5, E1.5, E.2.5 or E3.5 according to the desired embryonic
160 stage for collection. Embryos at E0.5 were collected after tearing of the
161 ampulla using a 30G needle in M2 medium supplemented with 10 µg/ml of
162 hyaluronidase. Embryos at E1.5 and E2.5 were collected after flushing the
163 oviduct via the infundibulum using M2 medium. Embryos at E3.5 were
164 collected after flushing the uterus with M2 medium and fixed immediately or
165 cultured up to E3.75, E4.0, E4.25 and E4.5 in KSOM medium at 37°C and 5%
166 CO2 prior to live imaging or fixation.

167

168 **Live imaging and time-lapse confocal microscopy**

169

170 Live imaging and time-lapse imaging of live embryos was performed in
171 a Quorum Spinning Disk Leica confocal microscope with the assistance of
172 Volocity software (Quorum Technologies, Guelph, ON, Canada). Embryos
173 were collected at different stages as described and placed in a M2 medium

drop on a Mat-Tek dish with glass bottom for immediate live imaging. For time-lapse imaging, embryos were placed in KSOM drops covered with mineral oil on a Mat-Tek dish at 37°C and 5% CO2. The live cell-imaging chamber (Chamlide, Live Cell Instrument, Namyangju-si, Korea) was placed on the microscope stage at least 30 minutes before placing the embryos, to equilibrate the system to 37°C and 5% CO2. Glass tips from pulled pipettes were used to contain the embryos and minimize embryo movement while imaging. Embryos were then placed in the chamber for time-lapse imaging. Time-lapse embryos were only imaged for 24-28h, in order to avoid discrepancies that could arise from cell death after prolonged UV exposure. Imaging was set for 1µm Z intervals, using maximum sample protection. Laser power and exposure times were set to the minimum value that yielded a robust eGFP signal (from 20-30 and 150-200ms, respectively) and sensitivity was set to the maximum level. Instant live imaging allowed longer exposure times to maximize eGFP signal.

Immunofluorescence of FGFR2-eGFP embryos

Embryos were retrieved from KSOM media and washed in M2 three times before fixation. Embryos were fixed with 4%PFA after 15 minutes of incubation at RT. PFA was prepared fresh daily or weekly and kept at 4°C. After fixation, embryos were washed in 3 drops of PBS (Ca2+ and Mg2+-free) supplemented with 1mg/ml of polyvinylpyrrolidone (PBS-PVP) and stored in PBS-PVP at 4C. Before immunostaining, we removed the zona pellucida by

briefly incubating embryos in acidic Tyrode's solution followed by rinsing in PBS-PVP supplemented with 1% BSA and 0.1% Triton X-100 (PBS-PVP-BSA). Embryos were then permeabilized for 15 minutes using PBS supplemented with 0.25% Triton X-100 in a Terasaki plate (Nunc, ThermoFisher). After permeabilization, embryos were rinsed three times in PBS-PV-BSA and incubated for 1h at RT in PBS-PVP supplemented with 10% donkey serum to block nonspecific antigens. Embryos were then incubated with primary antibodies diluted in PBS-PVP-BSA at 4°C overnight. Primary antibodies and their respective dilutions were as follows: mouse anti-GFP (Thermo Fisher, A11120, 1:100), rabbit anti-NANOG (Cell Signalling Technologies, 8822, 1:400), goat anti-GATA6 (R&D Systems, AF1700, 1:40) or goat anti-SOX17 (R&D Systems, AF1924, 1:400). On the next day, embryos were washed three times for 10 minutes in PBS-PVP-BSA and then incubated with secondary antibodies diluted in PBS-PVP-BSA for 1h at RT. Secondary antibodies and their respective dilutions were as follows: donkey anti-mouse Dy488 (Jackson, 715-485-151, 1:400), donkey anti-rabbit AF647 (Thermo Fisher, A31573, 1:400), donkey anti-goat AF546 (Thermo Fisher, A11056, 1:400). Embryos were washed three times for 10 minutes in PBS-PVP-BSA and incubated with Hoechst 33342 10 µg/ml in PBS-PVP-BSA for 10 minutes. Embryos were then rinsed three times in a 1:100 solution of Prolong live anti-fading reagent (P36975, ThermoFisher) diluted with PBS-PVP-BSA. Embryos were then placed into a drop of 5µl of Prolong Live anti-fading reagent solution on 100mm coverslips using an adhesive spacer (S24737, ThermoFisher), allowing different treatment or stages to remain in single drops. All immunostained embryos were evaluated under confocal

224 microscopy using a Quorum Spinning Disk Leica confocal microscope with
225 the assistance of Volocity software (Quorum Technologies, Guelph, ON,
226 Canada).
227
228 **Quantitative image analysis**
229 Immunostaining images were then analyzed by Image J software
230 (https://imagej.nih.gov/ij/; Schneider et al. 2012). Nuclei from the ICM were
231 identified and manually captured using the freehand selection tool at their
232 largest diameter. Fluorescence intensities were measured for all channels and
233 the decimal logarithmic value of mean pixel intensity was used for
234 downstream analysis. All intensities were plotted by respective Z stack and a
235 linear regression was performed to obtain the slope value. This slope value
236 was used to correct for fluorescence decay along the Z-axis as described
237 previously (22):
238 $Z\ Corrected\ Intensity = Original\ intensity - (Slope\ \times\ Z\ stack)$
239 Corrected values were then subtracted by an average of two
240 background values, which were also corrected by the Z-axis position. These
241 values were then used to correlate pixel intensity of GFP, NANOG and
242 GATA6 or SOX17 staining.
243
244
245 **Treatment with FGF or MEK inhibitor**
246
247 FGFR2-eGFP embryos collected at E2.5 were cultured in KSOM drops
248 at 37°C and 5% CO2. Embryos were untreated or treated with 500 ng/µl

FGF4 and 1 µg/ml heparin or 0.5mM MEK inhibitor PD325901 (MEKi) for 24h (E3.5), 30h (E3.75) or 48h (E4.5). Embryos were live imaged to observe FGFR2-eGFP or fixed and stained for NANOG and GATA6 as described above. GFP-positive cells in the ICM were counted using Image J.

Treatment with BMP4 or BMP inhibitors

FGFR2-eGFP embryos collected at E2.5 were cultured in KSOM drops at 37°C and 5% CO2. Embryos were left untreated or treated with 300 ng/ml BMP4 for 24h (E3.5), 30h (E3.75) or 48h (E4.5). Embryos were fixed and stained for NANOG, GATA6 or SOX17, and GFP as described above. NANOG and GATA6 or SOX17-positive cells were counted and fluorescence intensity of NANOG, GATA6 or SOX17 and GFP was measured in Image J as described above. In a different experiment, embryos were left untreated or treated with 500 nM (5Z)-7-oxozeaenol (7-oxo) or 1µM dorsomorphin (Dorso) from E2.5 to E4.5 (48h) and NANOG and SOX17-positive cells were counted.

Statistical analysis

Linear regression and Pearson correlation analysis were performed using GraphPad Prism7 software (GraphPad Software, Inc; San Diego, CA, USA). We analyzed cell count data by ANOVA using PROC GLM of SAS 9.4, considering embryos as subjects, treatments as the independent variable and cell count as a dependent variable, followed by Tukey's comparison of means. We also used PROC GLM of SAS 9.4 and Tukey's to analyze fluorescence

intensity, considering cells as subjects, treatments as independent variables and intensity as the dependent variable.

Results

Live dynamics of FGFR2 throughout pre-implantation development

We characterized the FGFR2-eGFP reporter expression by collecting embryos at different time points and performing live imaging using a spinning disk confocal. We observed green nuclear fluorescence beginning at E2.5 in some 8-cell stage embryos. However, some 8-cell embryos were still negative for eGFP, which suggested that FGFR2 expression starts at the late 8-cell stage. We observed eGFP expression at E3.0 in all outer cells of the morula stage and within a small number of inner cells. However, at E3.5, eGFP was only observed in the trophectoderm, while no clear nuclear localization of eGFP was observed in the inner cell mass (ICM). At E4.5, nuclear eGFP was seen in the ICM specifically in the cells closest to the blastocoel, where the PE cells lie (Figure 1).

Figure 1 - Dynamics of FGFR2-eGFP expression in mouse early embryo development. Representative images of homozygous FGFR2-eGFP embryos live imaged at E2.5, E3.0, E3.5 and E4.5. Embryos were staged based on morphology. Some 8-cell embryos were completely negative while others displayed positive cells. Nuclear eGFP is observed broadly by the morula stage. Early blastocysts display eGFP only in the TE, while expanded

298 blastocysts display GFP in ICM cells facing the blastocoel. Scale bar is equal
299 to 40µm.
300
301 To gain further insight on the dynamics of FGFR2-eGFP, we performed
302 time-lapse imaging of collected embryos. We imaged embryos from E1.5 to
303 E2.5, then E2.5 to E3.5 and E3.5 to E4.5. Time-lapse from E1.5 to E2.5
304 confirmed that nuclear eGFP appeared at late 8-cell stage (supplemental file
305 S3). From E2.5 to E3.5, most embryos had absent or reduced eGFP in inner
306 cells at the morula stage, leading to an ICM devoid of nuclear eGFP or with
307 few cells with very low eGFP intensity, especially when compared to the TE
308 (supplemental file S4). Similar observations were made when E3.5 was the
309 starting point, as most embryos still had little or weak GFP-positive cells in the
310 ICM but showed strong expression in the TE. After 12-16h in culture, a
311 stronger eGFP signal was observed in the ICM and after 24h it was possible
312 to observe the sorting of GFP-positive PE cells in the ICM (supplemental file
313 S5).
314
315 **Correlation between FGFR2, NANOG and GATA6**
316
317 Since there was no clear observation of eGFP-positive cells in the early
318 blastocyst, we decided to use a quantitative approach to assess if there is any
319 relationship between FGFR2 and NANOG or GATA6 protein expression. We
320 first grouped embryos by embryonic day: E3.5 (n=66 cells); E3.75 (n=125);
321 E4.0 (n=119); E4.25 (n=101) and E4.5 (n=107). Then we performed linear
322 regression analysis on data obtained by quantitative image analysis from

immunostaining of GFP, NANOG and GATA6 (Figure 2A). It is noticeable over time that the correlation values for GFP and NANOG become negative while GFP and GATA6 correlation values increase (Figure 2B). Pearson correlation analysis revealed an increase at E3.75, but overall it showed a decrease in the correlation of GFP and NANOG over time. Correlation between GFP and GATA6 increased as early as E3.75 and remained higher until E4.5 (Figure 2B). Pearson correlation analysis revealed a decrease in the correlation of NANOG and GATA6 over time, with the largest changes in correlation occurring at E3.75 and E4.25 (Figure 2B). Pearson correlation values and p-values are listed in Table 1. Linear regression analysis reveals the opposite trend in the relationship between NANOG or GATA6 with GFP (Figure 2C). We also plotted data based on NANOG and GATA6 fluorescence intensities. It was possible to observe a separation of cell populations over time, as cells were grouped in one cluster at E3.5 and two clusters can be observed at E4.25 and E4.5 (Figure 2D).

Figure 2 - Correlation of FGFR2-eGFP, NANOG and GATA6 based on embryonic day. A) Representative images of homozygous FGFR2-eGFP embryos at different embryonic days after immunostaining against GFP, NANOG and GATA6. Scale bar is equal to 40μm. B) Graphic representation of Pearson correlation values observed from E3.5 to E4.5. Blue dots represents GFP and NANOG correlation, red squares represent GFP and GATA6 correlation and green triangles represent NANOG and GATA6 correlation. C) Graphic representation of linear regression analysis of fluorescence intensity levels. Blue dots and blue line represents NANOG cell measurements and regression analysis considering NANOG and GFP levels

respectively. Red dots and red line represents GATA6 cell measurements and regression analysis considering GATA6 and GFP levels respectively. D) Dot plots depicting measured levels of NANOG and GATA6 in individual cells.

Table 1 - Pearson correlation values and respective two-tailed p-values of FGFR2-eGFP, NANOG and GATA6 fluorescence based on embryonic day.

	FGFR2eGFP: NANOG		FGFR2eGFP:GATA6		NANOG:GATA6	
	Pearson r	p-value	Pearson r	p-value	Pearson r	p-value
E3.5	-0,2195	0,0766	0,1272	0,3088	0,1723	0,1667
E3.75	-0,1261	0,161	0,721	< 0.0001	-0,3203	0,0003
E4.0	-0,3445	0,0001	0,4731	< 0.0001	-0,3503	< 0.0001
E4.25	-0,6554	< 0.0001	0,7593	< 0.0001	-0,76	< 0.0001
E4.5	-0,5599	< 0.0001	0,7445	< 0.0001	-0,5078	< 0.0001

We then grouped embryos based on embryo staging by cell number: 32-64 (n=111 cells); 65-90 (n=196); 91-120 (n=139) and 121-150 (n=65). Linear regression analysis was performed as above and as embryos grew larger, a similar trend was observed when compared to embryonic day staging. Pearson correlation analysis revealed a more linear decrease in correlation between GFP and NANOG and also a more linear increase in correlation between GFP and GATA6, again with the largest change occurring early, at the 65- to the 90-cell stage (Figure 3A). The correlation of NANOG and GATA6 also revealed a negative trend with the largest change occurring in 65 to 90-cell embryos (Figure 3A). Pearson correlation values and p-values based on embryo staging are listed in Table 2. Similar to data obtained by embryonic day grouping, linear regression analysis reveals the opposite trend

in the relationship between NANOG and GFP compared to GATA6 and GFP (Figure 3B). Again, we plotted data based on NANOG and GATA6 results and separation of the two cell populations occurred in 91 to 120-cell and 121 to 150-cell embryos (Figure 3C).

Figure 3 - Correlation of FGFR2-eGFP, NANOG and GATA6 based on cell number. A) Graphic representation of Pearson correlation values observed in embryos with 32 to 64 cells, 65 to 90 cells, 91-120 cells and 121-150 cells. Blue dots represents GFP and NANOG correlation, red squares represent GFP and GATA6 correlation and green triangles represent NANOG and GATA6 correlation. B) Graphic representation of linear regression analysis of fluorescence intensity levels. Blue dots and blue line represents NANOG cell measurements and regression analysis considering NANOG and GFP levels respectively. Red dots and red line represents GATA6 cell measurements and regression analysis considering GATA6 and GFP levels respectively. C) Dot plots depicting measured levels of NANOG and GATA6 in individual cells.

Table 2 - Pearson correlation values and respective two-tailed p-values of FGFR2-eGFP, NANOG and GATA6 fluorescence based on embryo cell number.

	FGFR2eGFP: NANOG		FGFR2eGFP:GATA6		NANOG:GATA6	
	Pearson r	p-value	Pearson r	p-value	Pearson r	p-value
32-64	0,01061	0,912	0,3617	< 0.0001	0,2847	0,0025
65-90	-0,1379	0,0539	0,6668	< 0.0001	-0,3606	< 0.0001
91-120	-0,4626	< 0.0001	0,6966	< 0.0001	-0,4901	< 0.0001
121-150	-0,4199	0,0005	0,8676	< 0.0001	-0,5447	< 0.0001

FGFR2 response to FGF or MEK inhibition

To assess the relationship between FGF4 signalling and FGFR2 we stimulated the FGF pathway or inhibited MEK signalling from E2.5 to E3.5, E3.75 or E4.5. We assessed live FGFR2-eGFP expression or NANOG and GATA6 expression by immunostaining. At E3.5, no FGFR2-eGFP was observed in the ICM in all three conditions (Figure 4A) Also, mutual expression of NANOG and GATA6 was observed in most of the cells in all three conditions (Figure 4B). At E3.75 and E4.5, GFP staining was weaker in MEKi-treated embryos (Figure 4A). FGF4 treated embryos displayed only GATA6 cells in the ICM, while MEKi treated embryos displayed only NANOG cells in the ICM, as expected (Figure 4B). We then counted FGFR2-eGFP-positive cells (E3.5 Control n=9 embryos, FGF4 n=8, MEKi n=12; E3.75 Control n=12, FGF4 n=11, MEKi n=4; E4.5 Control n=12, FGF4 n=8, MEKi n=10) and confirmed that FGF4 treatment increased FGFR2-eGFP cells from E3.75 onwards, and MEKi reduced the number of FGFR2-eGFP-positive cells at E4.5 (Figure 4C).

Figure 4 - Treatment of FGFR2-eGFP embryos with FGF4 or ERK inhibitor. A) Representative images of live imaged FGFR2-eGFP embryos at different embryonic days and consequently different exposure to treatment. Scale bar is equal to 47μm. B) Representative images of embryos immunostained for NANOG (grey) and GATA6 (red) at different embryonic days and consequently different exposure to treatment. Scale bar is equal to 47μm. C) Graphical display of GFP cell counts in the ICM at E3.5, E3.75 and

E4.5. Letters within each timepoint indicates statisitical significance, as "a" indicates significant differences from all other groups and "b" indicates significant differences from MEKi group.

FGFR2 response to BMP4 or BMP inhibition

We then opted to assess the effects of BMP4 on FGFR2 expression. BMP4 was added from E2.5 to E4.5. Embryos were fixed for immunostaining for GFP, NANOG and GATA6 from E3.5 to E3.75 or SOX17 at E4.5. Unlike FGF treatment, there is no drastic effect on the epiblast and PE cell population (Figure 5A). We then counted cells (Control n=11, BMP4 n=13 embryos) and observed a reduction in NANOG-positive cell numbers, although no increase in SOX17 cells (Figure 5C). We then performed quantitative image analysis (Control n=229 cells, BMP n=219 cells) from immunostaining and found that BMP increased fluorescence intensity of FGFR2-eGFP at 3.75 and E4.5 (Figure 5D). Pearson correlation analysis revealed that FGFR2-eGFP and SOX17 had a much higher correlation after BMP treatment (Figure 5B). Moreover, the negative correlation of FGFR2-eGFP and NANOG was more accentuated after BMP treatment (Figure 5B).

Figure 5 - Treatment of FGFR2-eGFP embryos with BMP4. A) Representative images of embryos from each experimental group after immunostaining for GFP, NANOG and SOX17. B) Graphic representation of Pearson correlation values between GFP, NANOG and SOX17 after BMP treatment. Blue lozenges represent values from Control group while red squares represent values from BMP treated group. C) Graphic representation

of cell counts in embryos after treatments for different times. D) Graphic representation of quantitative image analysis after immunostaining of GFP, NANOG and GATA6 or SOX17. Asterisk denotes significant statistical difference.

On the other hand, treatment with BMP signaling inhibitors (Control n=16 embryos, 7-oxo n=15, Dorsomorphin n= 16 embryos) did not change the numbers of NANOG-, SOX17- or FGFR2-eGFP-positive cells (Figure 6A and 6C). Quantitative image analysis (Control n=64 cells, 7-oxo n=61 cells, Dorso n=67 cells) revealed an increase in NANOG, SOX17, and FGFR2-eGFP fluorescence intensities after 7-oxo. Since this increase occurred in all three variables measured, the correlation between these variables followed the same trend in each treatment (Figure 6B), suggesting no effect of BMP inhibition on the differentiation of the PE.

Figure 6 - Treatment of FGFR2-eGFP embryos with BMP signaling inhibitors. A) Representative images of embryos from each treatment group at E4.5 after immunostaining for GFP, NANOG and SOX17. B) Graphic representation of Pearson correlation values between GFP, NANOG and SOX17 after BMP inhibitors treatment. Blue lozenges represent values from Control group, red squares represent values from 7- oxozeaenol treated group and green triangles represent values from dorsomorphin treated embroys. C) Graphic representation of cell counts in E4.5 embryos after different treatments. D) Graphic representation of quantitative image analysis after immunostaining of GFP, NANOG and SOX17. Different superscript letters denotes significant statistical difference between groups.

Discussion

Studying the segregation of epiblast and primitive endoderm can elucidate mechanisms of regulative development in mammalian embryos. MEK/ERK signaling stimulated by FGF is pivotal in determining cell fate within the ICM, leading to the specification of the PE (12). Using a transgenic mouse model expressing an eGFP reporter we observed the dynamics of FGFR2 expression during early embryo development, to correlate its expression with the segregation of the two ICM lineages.

Observing live embryos at different time points, we observed that expression of FGFR2 starts at the late 8-cell stage but does not include all cells at the 8-16 cell stage. By the blastocyst stage, the TE showed robust expression of FGFR2-GFP, consistent with its role in TE expansion and formation of the blastocoel (23). Interestingly, in the early blastocyst, none or very few cells in the ICM displayed FGFR2-eGFP; this contrasts with the reported E3.25 ICM Fgfr2 RNA expression data (15), suggesting a possible post-transcriptional regulation of Fgfr2 in ICM cells. FGFR2-eGFP only appeared in the ICM at later blastocyst stages. These results match with FGFR2 detection by immunofluorescence (24) and with another study using a FGFR2 fluorescent reporter (16)

Studies showed that deletion of *Fgfr1* impacted PE specification more severely than *Fgfr2* deletion, implicating that FGFR2 would be mainly involved with PE cell survival and proliferation (16,17). *Fgfr1*-null embryos treated with exogenous FGF4 did not recover PE formation, while *Fgfr2*-null embryos

could form PE after exogenous FGF4 treatment (16,17); this agrees with the absence or reduced presence of FGFR2-eGFP in early blastocysts, corroborating that FGFR2 indeed is secondary to FGFR1 in PE specification. In addition, a weak association of FGFR2-eGFP with GATA6 at the early blastocyst and the most significant increase in correlation between FGFR2-eGFP and GATA6 seen after the early blastocyst stage reiterates that FGFR2 is not the initial receptor for FGF4 signaling during PE specification. The developmental dynamics of the correlations between NANOG and FGFR2-eGFP or GATA6 and FGFR2-eGFP agree with the timing in which the number of double-positive cells starts to diminish and either NANOG- or GATA6-positive only cells emerge (25).

These data combined suggest an event or series of events that lead to these changes in the ICM from early blastocyst to the blastocyst stage. We decided to test if exogenous FGF4 stimulation or inhibition at earlier stages would affect FGFR2-eGFP expression in the early blastocyst. At E3.5, after 24h of treatment, no changes in FGFR2-eGFP were observed in embryos treated with FGF4 or MEK inhibitor, suggesting that the FGFR2 upregulation at the early blastocyst stage is independent of FGF signaling. This is corroborated by the fact that *Fgfr2* expression is unchanged in *Fgfr1*-null mice (17).

The data on the more prominent role of FGFR1 in PE specification does not undermine the importance of FGFR2 since *Fgfr2*-null mice present reduced number of PE cells in the ICM (16,17). The addition of FGFR2 may allow cells to have a more robust activation of ERK (26), leading to PE commitment. These data combined with the shift in correlation between

NANOG:GATA6 and GATA6:FGFR2-eGFP observed at E3.75 or 65-90 cells, prompted us to hypothesize that some other signaling molecule could induce FGFR2 expression.

Based on previous results (18,19), we tested if BMP signaling would be involved in regulating FGFR2 expression in this window of time. Results showed that FGFR2-eGFP was increased after BMP treatment at E3.75, although changes in EPI cell number were only observed at E4.5. No changes were observed from E2.5 to E3.5; this is in agreement with a proposed window of p38-MAPK activity soon after E3.5, which would ensure PE specification (27) through BMP signaling (18).

In summary, we observed that FGFR2 appeared at the late 8-cell stage, but its presence in the ICM of the early blastocyst is absent or reduced. As the blastocyst develops further, FGFR2 becomes expressed specifically in PE precursors within the ICM, as determined by the progressively increasing positive correlation with GATA6 expression and negative correlation with NANOG expression. Only this latest expression pattern is responsive to changes in overall FGF signaling levels. BMP stimulation also had little effect on EPI or PE cell numbers at earlier stages, only increasing FGFR2-eGFP from E3.75 onwards and reducing NANOG cells at E4.5. Thus, we conclude that FGFR2 is weakly associated with PE specification at the early blastocyst, but highly associated with PE lineage maintenance after the initial blastocyst stage.

Acknowledgements

Authors would like to thank Marina Gertsenstein and the Transgenic Core at Toronto Center for Phenogenomics for assistance in production of transgenic animals.

Funding Sources

This work was funded by CIHR Foundation grant # FDN-143334 to JR.

References

1. Lawrence PA, Levine M. Mosaic and regulative development: two faces of one coin. Curr Biol. 2006;16(7):236–9.
2. Gardner RL, Rossant J. Investigation of the fate of 4-5 day post-coitum mouse inner cell mass cells by blastocyst injection. J Embryol Exp Morphol. 1979;52:141–52.
3. Gardner RL. Investigation of cell lineage and differentiation in the extraembryonic endoderm of the mouse embryo. J Embryol Exp Morphol. 1982;68:175–98.
4. Chazaud C, Yamanaka Y, Pawson T, Rossant J. Early Lineage Segregation between Epiblast and Primitive Endoderm in Mouse Blastocysts through the Grb2-MAPK Pathway. Dev Cell. 2006;10(5):615–24.
5. Plusa B, Piliszek A, Frankenberg S, Artus J, Hadjantonakis A-K. Distinct sequential cell behaviours direct primitive endoderm formation in the

562 mouse blastocyst. Development. 2008;135(18):3081–91.
563 6. Niakan KK, Ji H, Maehr R, Vokes SA, Rodolfa KT, Sherwood RI, et al.
564 Sox17 promotes differentiation in mouse embryonic stem cells by
565 directly regulating extraembryonic gene expression and indirectly
566 antagonizing self-renewal. Genes Dev. 2010;24(3):312–26.
567 7. Kang M, Piliszek A, Artus J, Hadjantonakis A-K. FGF4 is required for
568 lineage restriction and salt-and-pepper distribution of primitive
569 endoderm factors but not their initial expression in the mouse.
570 Development [Internet]. 2013;140(2):267–79. Available from:
571 http://www.pubmedcentral.nih.gov/articlerender.fcgi?artid=3597205&too
572 l=pmcentrez&rendertype=abstract
573 8. Guo G, Huss M, Tong GQ, Wang C, Li Sun L, Clarke ND, et al.
574 Resolution of Cell Fate Decisions Revealed by Single-Cell Gene
575 Expression Analysis from Zygote to Blastocyst. Dev Cell [Internet].
576 2010;18(4):675–85. Available from:
577 http://dx.doi.org/10.1016/j.devcel.2010.02.012
578 9. Frankenberg S, Gerbe F, Bessonnard S, Belville C, Pouchin P, Bardot
579 O, et al. Primitive Endoderm Differentiates via a Three-Step Mechanism
580 Involving Nanog and RTK Signaling. Dev Cell. 2011;21(6):1005–13.
581 10. Schrode N, Saiz N, Di Talia S, Hadjantonakis AK. GATA6 levels
582 modulate primitive endoderm cell fate choice and timing in the mouse
583 blastocyst. Dev Cell. 2014;29(4):454–67.
584 11. Bessonnard S, De Mot L, Gonze D, Barriol M, Dennis C, Goldbeter A, et
585 al. Gata6, Nanog and Erk signaling control cell fate in the inner cell
586 mass through a tristable regulatory network. Development [Internet].

2014;141(19):3637–48. Available from:
http://www.ncbi.nlm.nih.gov/pubmed/25209243

12. Yamanaka Y, Lanner F, Rossant J. FGF signal-dependent segregation of primitive endoderm and epiblast in the mouse blastocyst. Development. 2010;137(5):715–24.

13. Kim SH, Kim MO, Cho YY, Yao K, Kim DJ, Jeong CH, et al. ERK1 phosphorylates Nanog to regulate protein stability and stem cell self-renewal. Stem Cell Res [Internet]. 2014;13(1):1–11. Available from: http://dx.doi.org/10.1016/j.scr.2014.04.001

14. Arman E, Haffner-Krausz R, Chen Y, Heath JK, Lonai P. Targeted disruption of fibroblast growth factor (FGF) receptor 2 suggests a role for FGF signaling in pregastrulation mammalian development. Proc Natl Acad Sci U S A [Internet]. 1998;95(9):5082–7. Available from: http://www.pubmedcentral.nih.gov/articlerender.fcgi?artid=20217&tool=pmcentrez&rendertype=abstract

15. Ohnishi Y, Huber W, Tsumura A, Kang M, Xenopoulos P, Kurimoto K, et al. Cell-to-cell expression variability followed by signal reinforcement progressively segregates early mouse lineages. Nat Cell Biol [Internet]. 2014;16(1):27–37. Available from: http://www.pubmedcentral.nih.gov/articlerender.fcgi?artid=4062977&tool=pmcentrez&rendertype=abstract

16. Molotkov A, Mazot P, Brewer JR, Cinalli RM, Soriano P. Distinct Requirements for FGFR1 and FGFR2 in Primitive Endoderm Development and Exit from Pluripotency. Dev Cell [Internet]. 2017;41(5):511-526.e4. Available from:

http://dx.doi.org/10.1016/j.devcel.2017.05.004

17. Kang M, Garg V, Hadjantonakis AK. Lineage Establishment and Progression within the Inner Cell Mass of the Mouse Blastocyst Requires FGFR1 and FGFR2. Dev Cell [Internet]. 2017;41(5):496-510.e5. Available from: http://dx.doi.org/10.1016/j.devcel.2017.05.003

18. Thamodaran V, Bruce AW. p38 (Mapk14/11) occupies a regulatory node governing entry into primitive endoderm differentiation during preimplantation mouse embryo development. Open Biol [Internet]. 2016;6(9):160190. Available from: http://www.ncbi.nlm.nih.gov/pubmed/27605380%0Ahttp://www.pubmedcentral.nih.gov/articlerender.fcgi?artid=PMC5043583%0Ahttp://www.ncbi.nlm.nih.gov/pubmed/27605380%5Cnhttp://rsob.royalsocietypublishing.org/lookup/doi/10.1098/rsob.160190

19. Graham SJL, Wicher KB, Jedrusik A, Guo G, Herath W, Robson P, et al. BMP signalling regulates the pre-implantation development of extra-embryonic cell lineages in the mouse embryo. Nat Commun [Internet]. 2014;5(May):5667. Available from: http://www.nature.com/doifinder/10.1038/ncomms6667

20. George SHL, Gertsenstein M, Vintersten K, Korets-Smith E, Murphy J, Stevens ME, et al. Developmental and adult phenotyping directly from mutant embryonic stem cells. Proc Natl Acad Sci [Internet]. 2007 Mar 13;104(11):4455–60. Available from: https://pnas.org/doi/full/10.1073/pnas.0609277104

21. Rodríguez CI, Buchholz F, Galloway J, Sequerra R, Kasper J, Ayala R, et al. High-efficiency deleter mice show that FLPe is an alternative to

637 Cre-loxP. Nat Genet [Internet]. 2000 Jun;25(2):139–40. Available from:
638 http://www.nature.com/articles/ng0600_139
639 22. Saiz N, Kang M, Schrode N, Lou X, Hadjantonakis A-K. Quantitative
640 Analysis of Protein Expression to Study Lineage Specification in Mouse
641 Preimplantation Embryos. J Vis Exp [Internet]. 2016;(108):1–13.
642 Available from: http://www.jove.com/video/53654/quantitative-analysis-
643 protein-expression-to-study-lineage
644 23. Yang J, Zhang D, Yu Y, Zhang RJ, Hu XL, Huang HF, et al. Binding of
645 FGF2 to FGFR2 in an autocrine mode in trophectoderm cells is
646 indispensable for mouse blastocyst formation through PKC-p38
647 pathway. Cell Cycle. 2015;14(20):3318–30.
648 24. Haffner-Krausz R, Gorivodsky M, Chen Y, Lonai P. Expression of Fgfr2
649 in the early mouse embryo indicates its involvement in preimplantation
650 development. Mech Dev. 1999;85(1–2):167–72.
651 25. Saiz N, Mora-Bitrià L, Rahman S, George H, Herder JP, García-Ojalvo
652 J, et al. Growth factor-mediated coupling between lineage size and cell
653 fate choice underlies robustness of mammalian development. Elife.
654 2020;9:1–38.
655 26. Simon CS, Rahman S, Raina D, Schröter C, Hadjantonakis AK. Live
656 Visualization of ERK Activity in the Mouse Blastocyst Reveals Lineage-
657 Specific Signaling Dynamics. Dev Cell. 2020;55(3):341-353.e5.
658 27. Bora P, Gahurova L, Mašek T, Hauserova A, Potěšil D, Jansova D, et
659 al. p38-MAPK-mediated translation regulation during early blastocyst
660 development is required for primitive endoderm differentiation in mice.
661 Commun Biol. 2021;4(1):788.

Supplemental file legends

S1 file - DNA sequence of the plasmid used for homologous recombination in ES cells

S2 file - Schematic representation of the plasmid used for homologous recombination in ES cells

S3 file - Time-lapse imaging of live FGFR2-eGFP embryos from E1.5 to E2.5

S4 file - Time-lapse imaging of live FGFR2-eGFP embryos from E2.5 to E3.5

S5 file - Time-lapse imaging of live FGFR2-eGFP embryos from E3.5 to E4.5

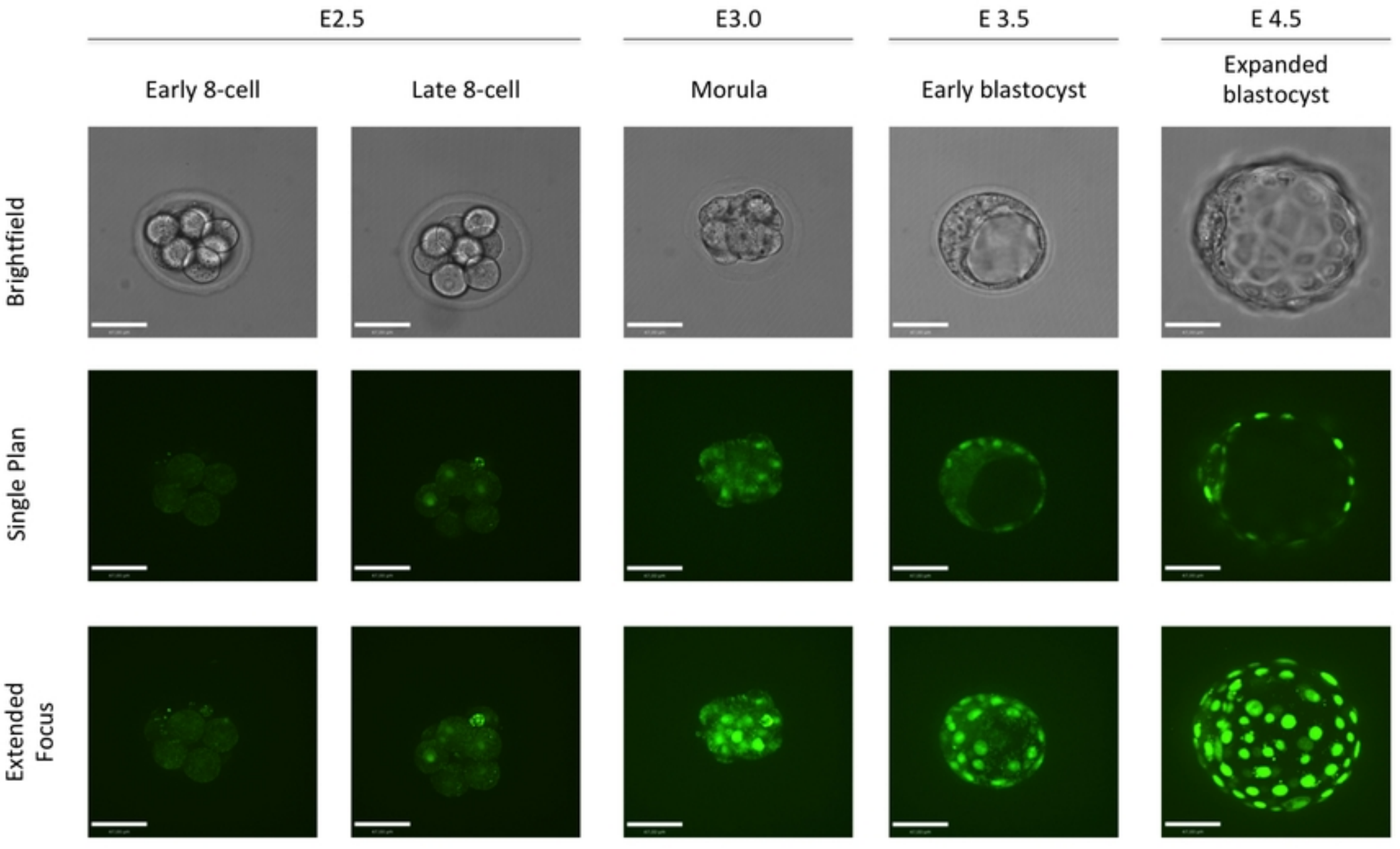
E2.5
E3.0
E 3.5
E 4.5
Early 8-cell
Late 8-cell
Morula
Early blastocyst
Expanded blastocyst
Brightfield
Single Plan
Extended Focus

Figure 1

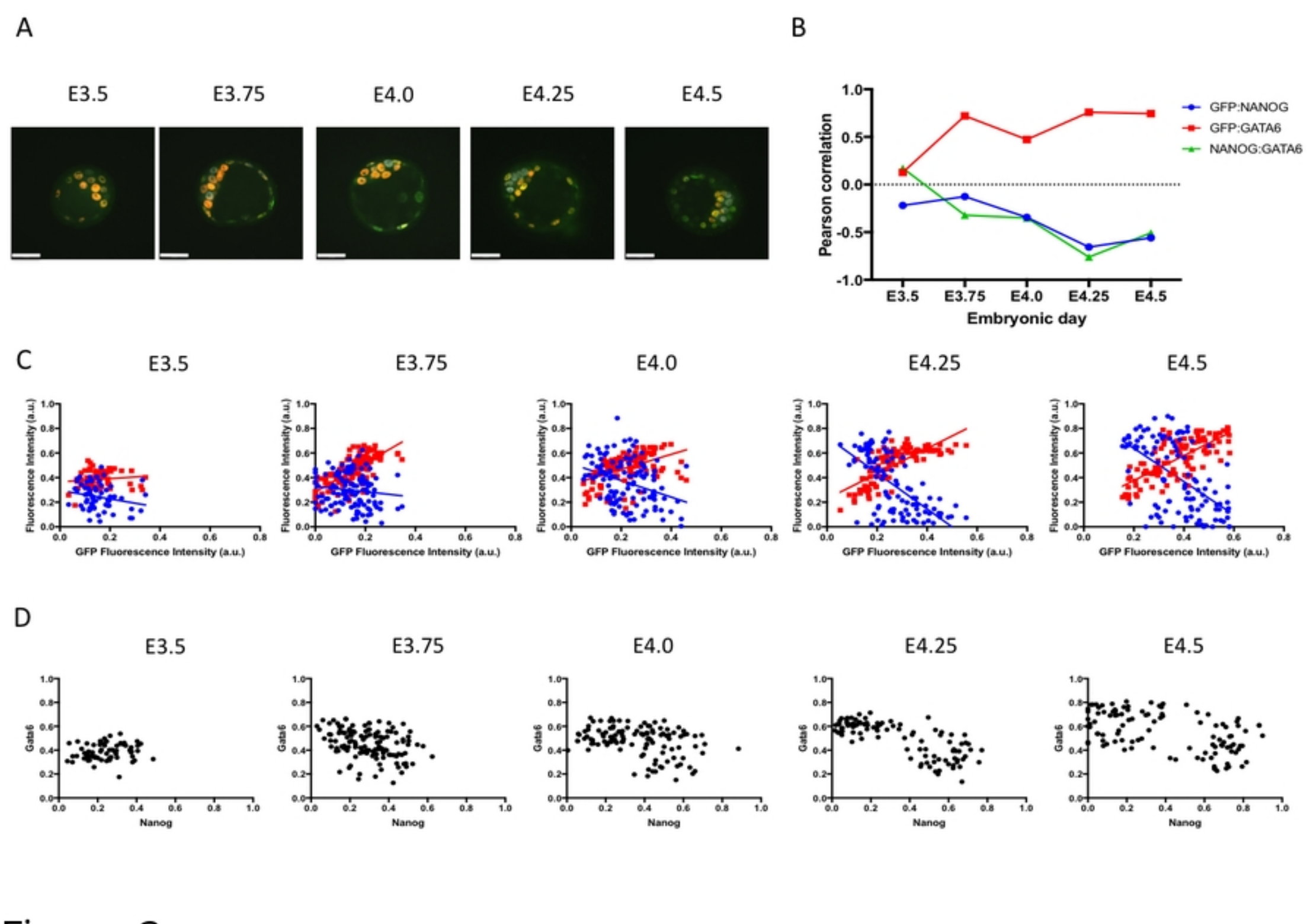
A
E3.5
E3.75
E4.0
E4.25
E4.5
B
Pearson correlation
1.0
0.5
0.0
-0.5
-1.0
E3.5
E3.75
E4.0
E4.25
E4.5
Embryonic day
GFP:NANOG
GFP:GATA6
NANOG:GATA6
C
E3.5
E3.75
E4.0
E4.25
E4.5
Fluorescence Intensity (a.u.)
GFP Fluorescence Intensity (a.u.)
D
E3.5
E3.75
E4.0
E4.25
E4.5
Gata6
Nanog

Figure 2

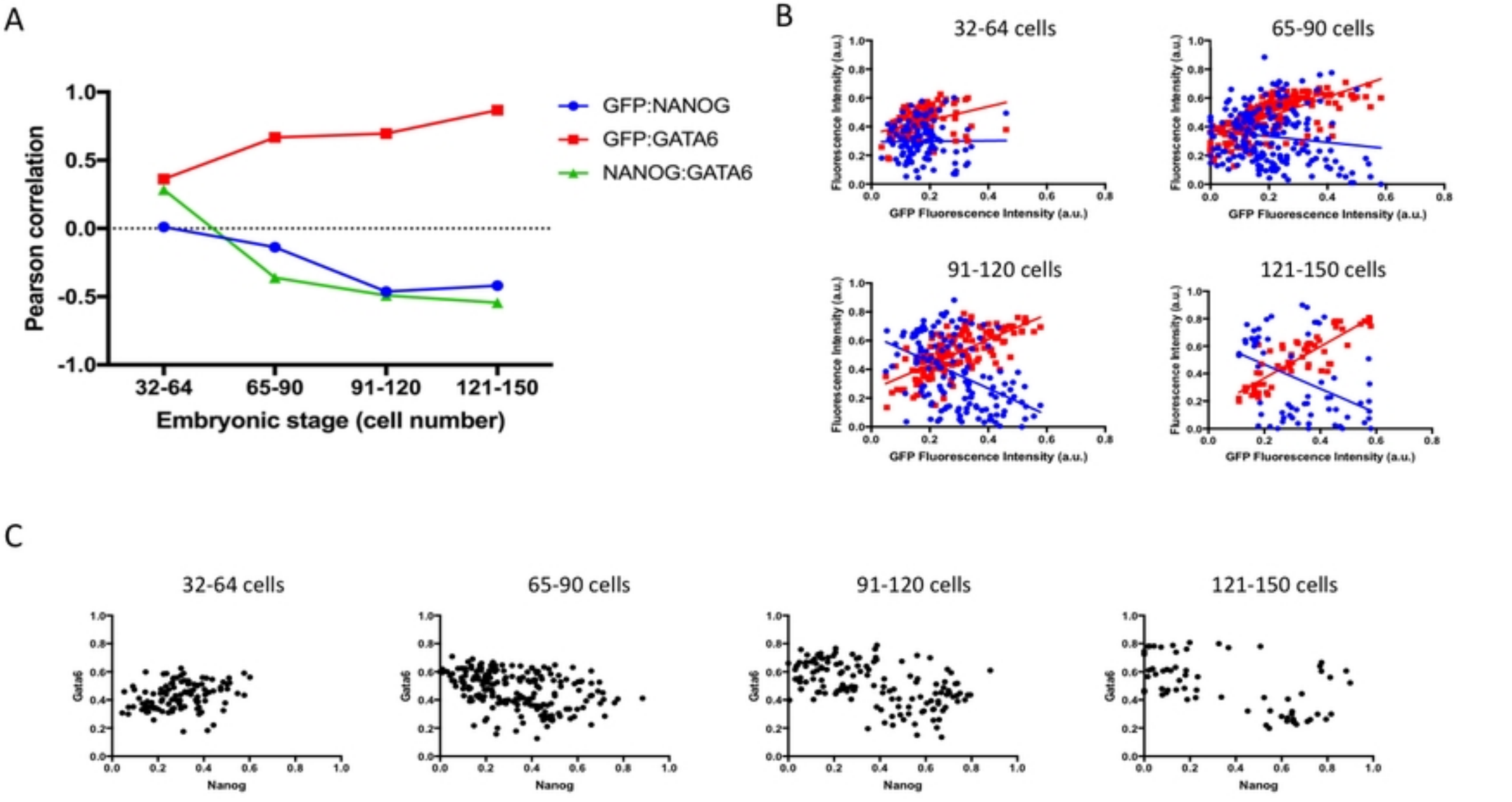
A
Pearson correlation
1.0
0.5
0.0
-0.5
-1.0
32-64
65-90
91-120
121-150
Embryonic stage (cell number)
GFP:NANOG
GFP:GATA6
NANOG:GATA6
B
32-64 cells
65-90 cells
91-120 cells
121-150 cells
Fluorescence Intensity (a.u.)
GFP Fluorescence Intensity (a.u.)
C
32-64 cells
65-90 cells
91-120 cells
121-150 cells
Gata6
Nanog

Figure 3

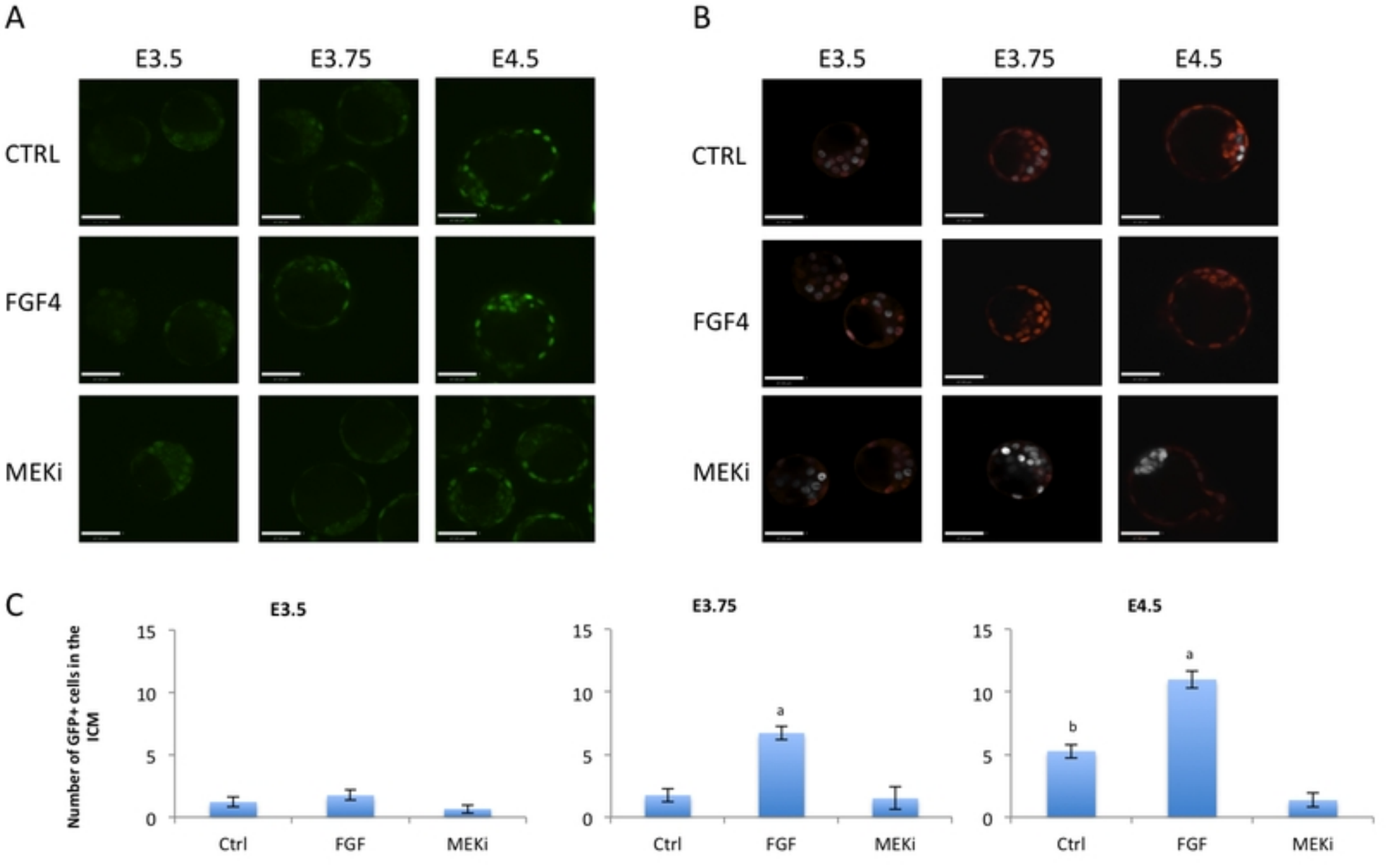
A
E3.5
E3.75
E4.5
CTRL
FGF4
MEKi
B
E3.5
E3.75
E4.5
CTRL
FGF4
MEKi
C
E3.5
E3.75
E4.5
Number of GFP+ cells in the ICM
15
10
5
0
Ctrl
FGF
MEKi
a
b

Figure 4

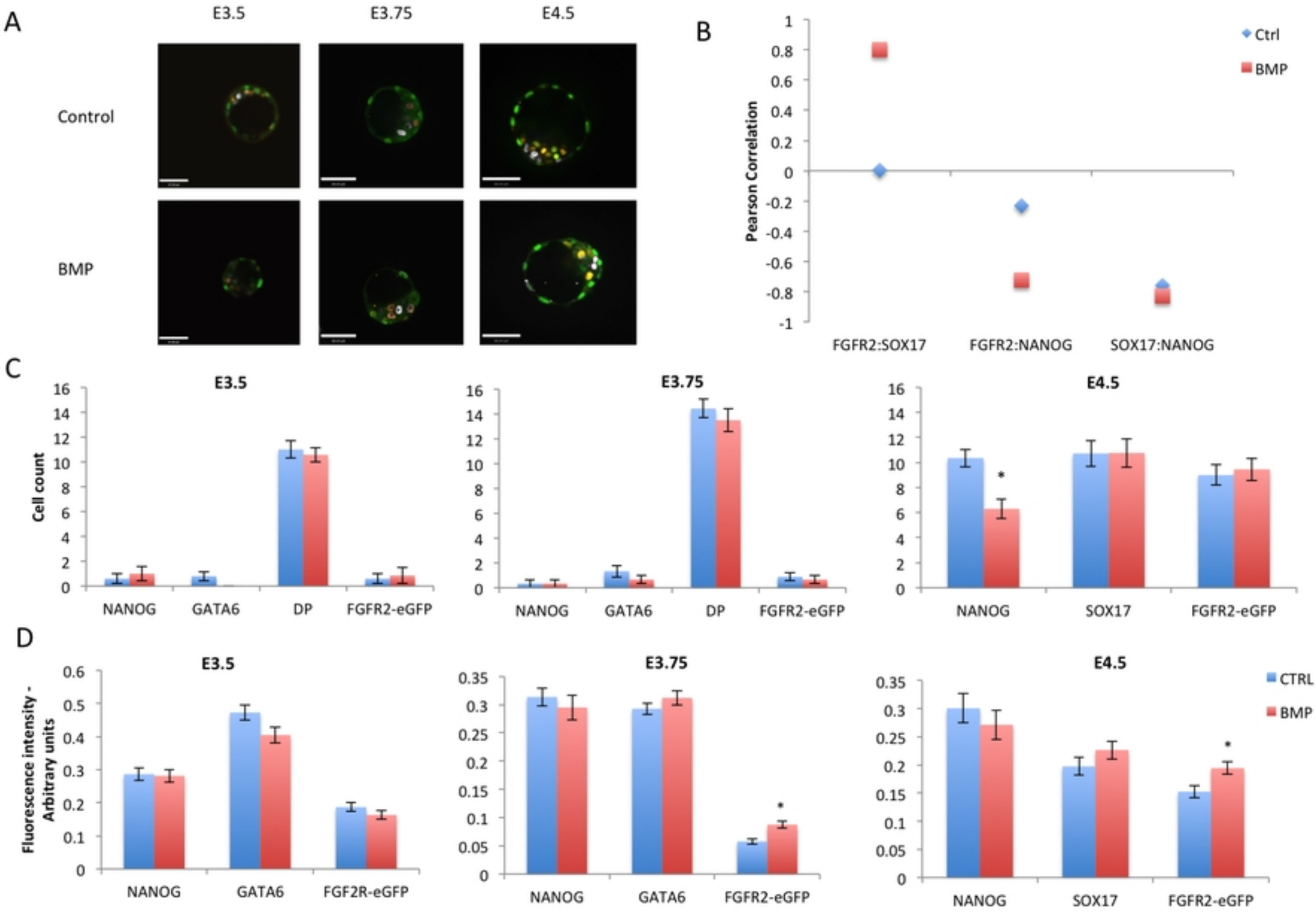
A
E3.5
E3.75
E4.5
Control
BMP
B
Ctrl
BMP
Pearson Correlation
1
0.8
0.6
0.4
0.2
0
-0.2
-0.4
-0.6
-0.8
-1
FGFR2:SOX17
FGFR2:NANOG
SOX17:NANOG
C
E3.5
E3.75
E4.5
Cell count
NANOG
GATA6
DP
FGFR2-eGFP
SOX17
D
Fluorescence intensity - Arbitrary units
FGF2R-eGFP
CTRL
BMP

Figure 5

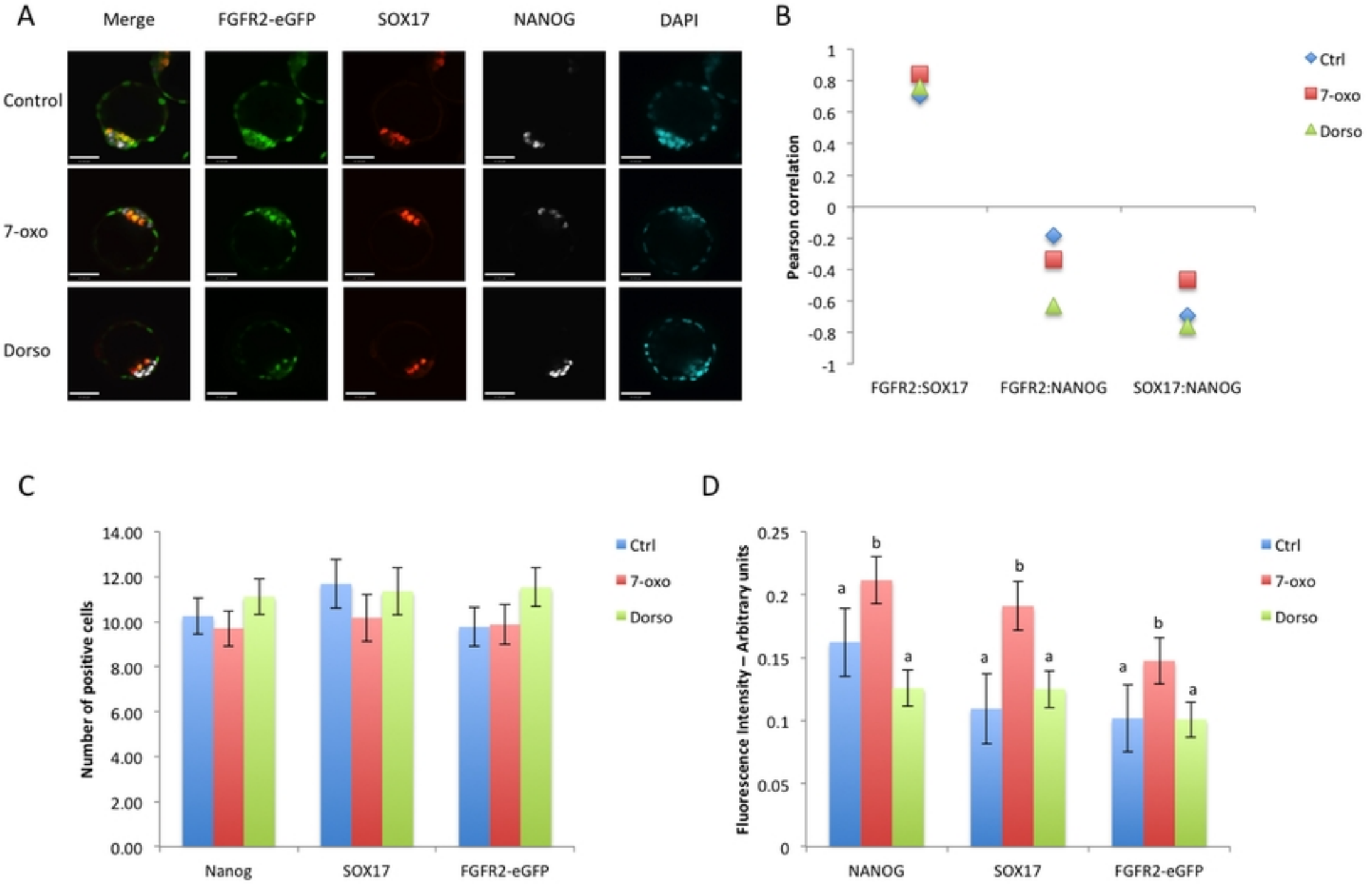
A
Merge
FGFR2-eGFP
SOX17
NANOG
DAPI
Control
7-oxo
Dorso
B
Pearson correlation
1
0.8
0.6
0.4
0.2
0
-0.2
-0.4
-0.6
-0.8
-1
FGFR2:SOX17
FGFR2:NANOG
SOX17:NANOG
Ctrl
7-oxo
Dorso
C
Number of positive cells
14.00
12.00
10.00
8.00
6.00
4.00
2.00
0.00
Nanog
SOX17
FGFR2-eGFP
Ctrl
7-oxo
Dorso
D
Fluorescence Intensity – Arbitrary units
0.25
0.2
0.15
0.1
0.05
0
a
b
a
a
b
a
a
b
a
NANOG
SOX17
FGFR2-eGFP
Ctrl
7-oxo
Dorso

Figure 6